

Adaptive Airfoils For Helicopter Control

RL Roglin, SV Hanagud, SKondor

Georgia Institute of Technology
School of Aerospace Engineering

ABSTRACT

This paper discusses the development of a new helicopter rotor system. The aspect of this rotor system which is new is the replacement of the collective control with rotor blades which generate lift by a camber change. The initial work could only produce a camber change in an on / off fashion where the camber change was of a fixed magnitude. This work includes the development of a control scheme which allows a number of different camber changes.

1.0 INTRODUCTION:

The development of an intelligent structure requires three components. These components are sensors to determine the current state of the structure, actuators to alter the structure from the current state to a desired state, and an algorithm to determine what the desired state of the structure should be. When these three components are present and functional in a structure this structure will have the ability to interact with its environment as the environment is perturbed. The key being the ability to interact according to a predetermined set of rules. An example is an aeroelastically tailored wing. Where the torsional stiffness of the wing is coupled with the bending stiffness to increase the speed when torsional divergence will occur.

The adaptive airfoil presented in this paper includes all three of the required components. The sensor package consists of four strain gages located along the span of the blade. The actuator drives a trailing edge flap which changes the camber of a portion of the main rotor blade. The algorithm compares the output from the sensors on blade 1 and blade 2. Based on this comparison the power distribution to the actuator is altered to increase the camber of one blade and decrease the camber of the other blade. This comparison / distribution loop is repeated till the blades are tracking correctly.

2.0 SHAPE MEMORY ALLOYS:

In 1965 at the U.S. Naval Ordnance Laboratory Beuhler and Wiley received a United States Patent for a series of engineering alloys that possessed a unique mechanical "memory", generically named 55-Nitinol due to the fact that the material contains approximately 55 weight percent nickel in chemical composition. The Naval Ordnance Laboratory now called the Naval Surface Warfare Center has been very active in characterization of this material. Other laboratories including Battelle-Memorial Institute and National Aeronautics and Space Administration have also made major contributions toward understanding the mechanism associated with shape memory alloys (SMA).

Figure 1 illustrates the formation of Martensite in a shape memory alloy and the relationship between temperature and the geometric properties of length and volume and the material property of electrical resistance.

Fundamental to the shape memory effect is the occurrence of a martensitic phase transformation and its subsequent reversal. During the martensitic phase the material is soft and easy to deform. The shape memory effect occurs when the specimen is heated and undergoes the phase transformation to its parent or austenitic state. Relatively large strains (6% to 10%) can be achieved with

these alloys making them a candidate for actuation type applications.

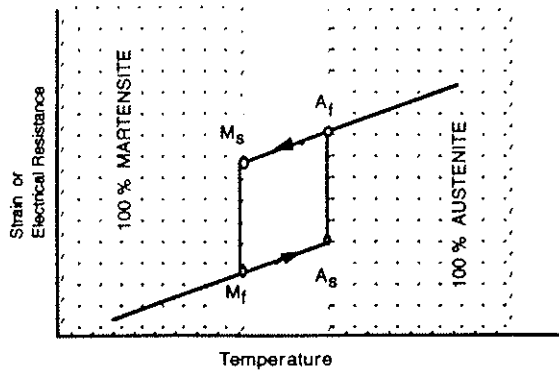


Figure 1. Strain vs. Temperature

This phenomenon of shape memory or the shape memory effect (SME) is illustrated in Figure 2. Let us consider a wire made of SMA (Step 1). Let us also assume that this wire is stretched and deformed inelastically at low temperature (Step 2). The wire is then heated to a temperature above a certain critical temperature (Step 3) to determine the shape that is to be remembered and then cooled. A mechanical stress is then applied to deform the cool wire (STEP 4). Then heat the wire and it returns to its remembered geometric shape (Step 5).

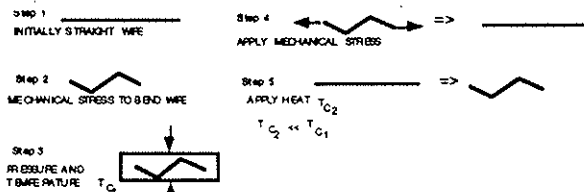


Figure 2. The shape memory effect

Although the shape memory phenomena was first investigated in the 1960's and the shape memory effect has been seen in different alloys only three alloys which exhibit this phenomena are presently in commercial use CuZnAl, CuAlNi, and NiTi

Many researchers were involved in determining the mechanism which explains these alloys unique abilities. These alloys have the mechanical ability to accommodate plastic strains of typically six to eight percent and when restrained from regaining their

original shape they can generate stresses in the range of 100,000 psi. These force and displacement capabilities make shape memory alloys an attractive material for electromechanical actuators.

The shape memory effect results from the formation of martensitic plates. Figure 3 illustrates a single plane of shape memory alloy. In the austenitic phase or parent phase the plane has the shape of a square (this is the shape which has been memorized by the material as described in figure 2).

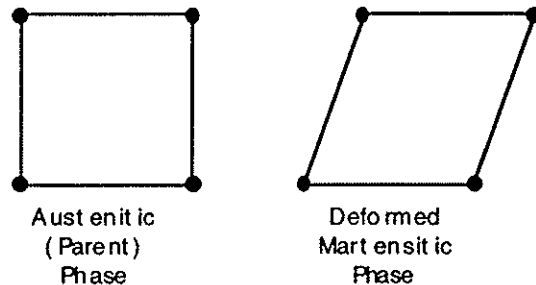


Figure 3. Austenitic / Martensitic planes

When the alloy is at a temperature below M_f it is deformed into a rhombus. When the alloy is cooled below M_f martensitic plates form which are self-accommodating and cause no macroscopic deformations. the plane is then deformed into a rhombus under a mechanical load which is subsequently removed. When the alloy is then heated the martensitic plates begin to disappear starting at A_s and by the time the alloy has reached A_f all the martensitic plates are gone and the shape of the plane is back to that of a square.

In two dimensions there are four ways the square can be deformed into the rhombus illustrated in Figure 4. Once a path of deformation has been established for deforming the plane from a square to a rhombus this is the only path that can be followed. This means that if the square has been deformed by application of a shear along the top surface as seen in Figure 4a the reverse process will be for the top to slide back to the left.

The characteristic of self-accommodation demonstrated by the martensitic plates causes four of the rhombic variants to group together. Figure 5 illustrates this grouping in the large scale picture of a specimen ABCD under a load acting to the upper right. In this orientation three of the rhomboids are unstable (1, 3, and 4) with respect to the stress. these three will be consumed by the growth of martensitic plates in rhombus number 2. When this specimen is subsequently heated the martensitic plates formed will disappear and the shape will follow the reverse of the deformation path to return to it's original square shape.

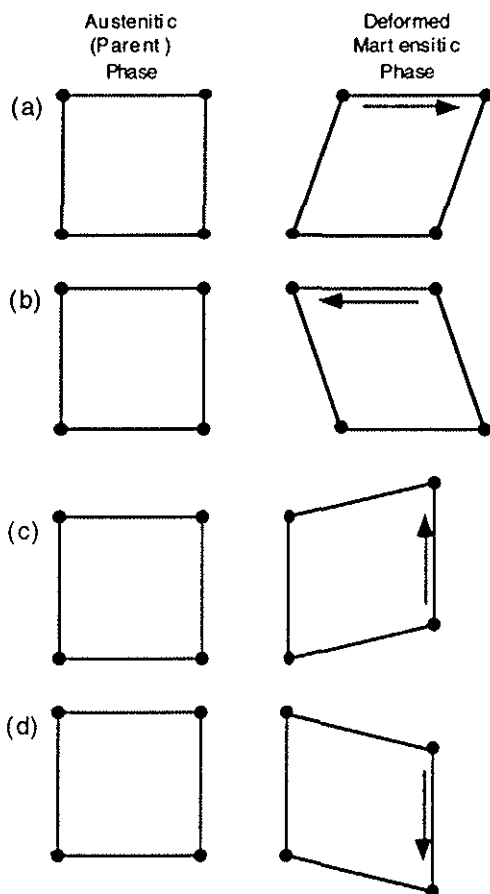


Figure 4. Deformation paths

This phenomena is described as the one way shape memory effect because after the specimen is heat and returns to it's

original shape it will remain in this shape under temperature cycling. The specimen can be deformed again in the martensitic phase and will return to the parent shape when heated above the austenitic start temperature. Therefore as long as there is a stress to deform the specimen in the martensitic phase the material can be cycled.

The temperature deformation relationship is illustrated in Figure 1. In this figure there is a transition temperature where the alloy undergoes a material phase transformation from austenite to martensite it is this phase transformation which is responsible for the shape memory effect. The effect of the end conditions is illustrated in Figure 6. As the end condition stiffness change from free to fixed the deformation of a wire specimen decreases and internal specimen stress increases this can lead to a phenomenon known as stress induced martensitic transformation of the alloy.

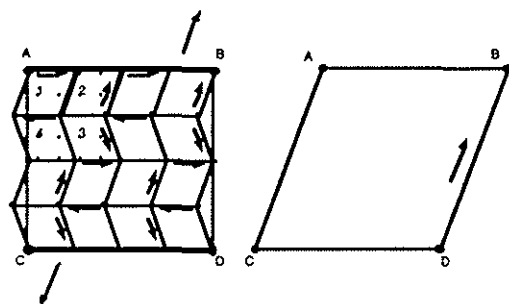


Figure 5. Self-accommodation of martensitic plates

The fabrication of SMA hybrid composites are an example of a material with "Intelligence at the most primitive levels". These composite materials contain a lamina of SMA fibers. There is still much to be learned about the interaction of stress and temperature in relation to the extent, reliability and fatigue life of shape memory alloy dynamic actuators. Composite materials which incorporate shape memory fibers have tremendous potential for creating structures which can adapt to changes in their loading environment . When these composite materials are heated they can demonstrate stiffness increases of as much as three times

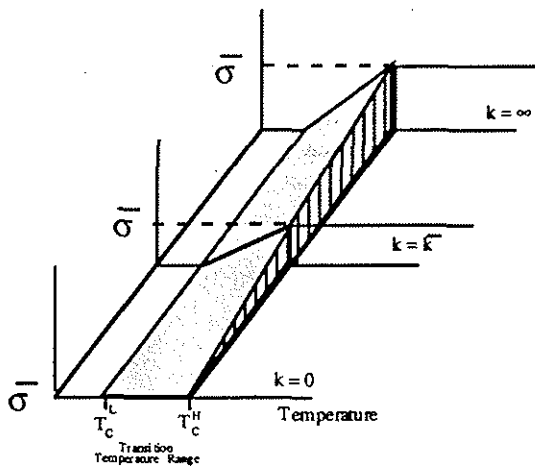
that of the unheated material. There are many applications for such an actuator. These include vibration control through the processes of active stiffness tuning or active strain energy tuning.

Active stiffness tuning is a method of steady state vibration control. The vibration characteristics, frequencies and mode shapes, of a structure or mechanical component can be altered in a controlled fashion by heating the embedded or bonded shape memory alloy fibers associated with the structure. As the fibers heat the alloy experiences a phase change when it transforms from the martensitic state to an austenitic state. Associated with this phase transformation is an increase in Young's

increases will result in a stiffer structure with higher natural frequencies.

Active strain energy tuning is a process in which a shape memory lamina is located and oriented in such a way that upon heating it will not deform the structure but instead will impose a residual state of strain. The resulting stored strain energy (compression or tension) changes the total energy distribution and modifies the modal response of the structure .

There are limitations associated with this material when it is used to control structural vibrations. First, note that the contraction of this material is solely due to heating and the relaxation is solely due to cooling. To achieve the maximum frequency response requires an active control loop which will monitor the material temperature. The minimum temperature must not be allowed to be less than the martensite finish temperature and the maximum temperature must not be allowed to exceed the austenite finish temperature. This means the temperature must be kept in a range of 40° C for material with a transition temperature of 90° C. The other limitation is the inertia effect. This effect is present when the material is rapidly contracted with an external load such as in the case of a wire actuator. Under these conditions the inertia effect associated with the load which the actuator is attempting to move can overstress the wire actuator. A practical frequency response of 4 hertz can be achieved for a wire with a diameter of 0.010 inches if the wire is heated using short (millisecond) high bursts of current and cooled using a water with glycol bath . This type actuator will require very high values of current to heat the wire since an active cooling mechanism (a water with glycol bath) is being used to continuously remove heat from the wire.



Temperature Relationship

$$\sigma = \bar{\sigma} \left(\frac{T - T_C^L}{T_C^H - T_C^L} \right)$$

Deformation Relationship

$$\delta = 0 \Rightarrow k = \infty : \bar{\sigma} = \sigma_{\max}$$

$$\delta = \delta_{\max} \Rightarrow k = 0 : \bar{\sigma} = 0$$

$$\bar{\sigma} = \sigma_{\max} \left(\frac{\delta_{\max} - \delta}{\delta_{\max}} \right)$$

Figure 6. End condition effect

modulus by a factor of three and an increase in yield strength by a factor of ten. Since the natural frequencies of any structure are proportional to the Young's modulus these

The application to structural mechanics problems of these hybrid shape memory alloy composites is far greater than just the control of vibrations. The ability of the material to change modulus of elasticity would allow discretely placed shape memory

alloy fibers to increase the critical buckling load of flexible structures or alter the critical speed of a flexible drive shaft. Another area where shape memory alloys will excel is in shape control of flexible structures. This application will include both motion and shape control. To accomplish this a controller must simultaneously employ force actuators and stiffness actuators for transition to occur from one predetermined shape to another similar to the way the human muscular system works.

3.0 CONTROL PROBLEMS:

The environment in which a helicopter must operate is extremely complex due to the interaction between the vehicle dynamics and the aerodynamic loading. The low natural frequencies associated with the rotor blades result in severe dynamic loading of the fuselage through the rotor hub. In addition to the aerodynamic loading of the rotor system there are also the additional forces associated with any rotating system. These include centrifugal, coriolis, and gyroscopic forces. In forward flight the rotational system is also subject to an asymmetrical lift due to differences in the airflow over the advancing and retreating blades. The aeroelastic phenomena described above combine to result in an aerodynamic flow around the rotor disk which is unsteady and asymmetric with airloads changing periodically along the span due to variations in blade section velocity and deformation.

Solutions to reduce the impact of asymmetrical loads and the resulting rotor blade vibration have been proposed and implemented in the following three areas.

- Alterations to blade and hub systems
- Passive vibration control schemes
- Active vibration control schemes

The first area is to improve the blade and hub systems. These include new blade airfoil sections or tips and elastomeric rotor hubs. With these solutions engineers are attempting to eliminate the unwanted vibratory effects before they enter the

fuselage. There are drawbacks associated with this solution. First, they are applicable in a limited portion of the flight envelope and second, it is extremely expensive to manufacture a blade in which the cross section (airfoil shape) varies from root to tip.

The second area is to incorporate passive devices to isolate the pilot, passengers, or cargo from the effects associated with the vibratory loading. The problem with this solution is there is usually a weight penalty associated with these isolation devices and the devices usually have a narrow range of vibratory loading for which they are effective.

The third area is the employment of active vibration control schemes. These schemes can be developed to have flexibility in how they modify the rotor system response characteristics. Higher harmonic control and individual blade control are two examples of active control schemes.

The higher harmonic control scheme is based on the fact that the vibratory loads acting on the blade are harmonic in nature and contain an infinite number of harmonic components. Normally, the swashplate inputs (changes in rotor blade pitch or angle of attack) which are applied to the rotor system only address the phenomena associated with the lower harmonics such as lift, thrust, and trim forces. But in this scheme collective and cyclic inputs are supplemented by additional higher harmonic inputs which interact with the airloads to reduce vibration of the rotor system. The drawbacks of this scheme are:

- There must be sufficient control force to overcome the mass inertia effect associated with the swashplate and pitch links.
- The swashplate must be stiffer to transfer the forces associated with a smaller stroke or tilt of the plate as would occur when transmitting a higher harmonic inputs.

- Each blade at a given azimuthal location is constrained to follow the same pitch variation.

The individual blade control scheme differs from the higher harmonic control scheme in that the control mechanism is now associated with each rotor blade at the blade level rather than at the rotor hub level. This means that each blade has the ability to act independently of the other blades thus allowing the implementation of more complex control inputs to the rotating system. Alterations of the rotor blade dynamic characteristics now have another degree of freedom associated with the problem of reducing vibratory loads before they enter the rotor hub. The current method of washplate stroke and tilt for collective and cyclic control inputs can now be eliminated if these basic rotor functions of lift, thrust generation, and trim are moved to the rotor blade.

4.0 CURRENT WORK:

The objective of this research was to investigate the application of an adaptive material as an actuation mechanism for individual blade collective control. This actuator was employed to change the camber of a portion of the main rotor blade. The primary function of this camber change was to generate thrust and replace the collective control currently used to generate thrust. The unique features of this work are:

- The use of an **ADAPTIVE MATERIAL** as the actuation element of the electromechanical actuator in an individual blade collective control scheme which will change the camber of an airfoil
- Employment of camber change as the **PRIMARY** thrust generating mechanism in a powered lift vehicle

The motivations for pursuing this problem were the potential improvement to performance by implementation of individual blade control to alter of the cross section shape and blade twist, the potential improvements to reliability through reduction

in the number of moving parts and maintainability through a reduction in the mechanical complexity of the actuation system.

The accomplishments associated with the research are the design, fabrication and testing of a flight vehicle. The design tasks dealt with how to modify the power plant of an existing internal combustion powered helicopter and the design of a control surface to be incorporated into the main rotor blades. The fabrication task was then the manufacturing of the required parts to transfer the design concept from paper to hardware. The testing task involved both ground and flight test of the modified vehicle to insure the structure integrity of the modifications. Finally the feasibility of the idea was demonstrated in flight test when a deflection of the control surface by an adaptive material resulted in vertical climb of the helicopter.

4.1 *Helicopter*

This project started with a generic radio controlled helicopter. A three view of the helicopter and the characteristic data associated with the helicopter are shown in Figure 7. The recommended internal combustion motor to be used with a helicopter of this size has an output of 1.8 horsepower and can generate 17,000 rpm under load.

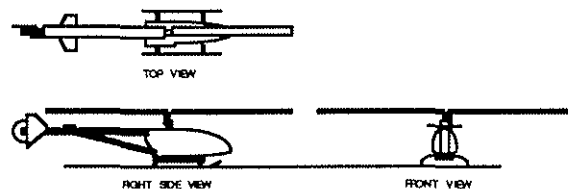


FIGURE 7 Three View

Fuselage Length	35 in
Fuselage Width	8 in
Helicopter Weight	108 oz
Power Plant Weight	20 oz

PARAMETERS	MAIN	TAIL
Radius	28 in	6 in
Chord	2.5 in	0.75 in
Solidity	0.0568	0.0796

No. of Blades	2	2
Tip Speed	4693 in/sec	4023 in/sec
Airfoil Section	NACA 0012	NACA 0012
Collective Range	+8° -> -8°	+8° -> -8°
Long Cyclic Range	+5° -> -5°	N/A
Lateral Cyclic Range	+5° -> -5°	N/A

Control of this helicopter is achieved with five small servo actuators. These function as follows:

- Longitudinal Cyclic
- Lateral Cyclic
- Collective Main Rotor
- Collective Tail Rotor
- Throttle

There is mechanical coupling between the main rotor collective and lateral cyclic and electronic coupling between the main rotor collective, tail rotor collective and throttle.

4.2 Helicopter Modifications

This baseline helicopter was then modified to remove the internal combustion power plant and incorporate an electric power plant. The reason for this modification was to improve the reliability and repeatability of helicopter flights. The internal combustion motors are sensitive to many factors such as fuel content and carburetor adjustments. This sensitivity results in many hours of downtime spent diagnosing and correcting power plant problems. This sensitivity also leads to variations in the power available and the associated performance of the helicopter which adversely effect the repeatability of the experimental results. There is also the problem of testing the helicopter indoors with an internal combustion power plant. Since volatile liquid fuels are used there is a real possibility of fire or explosion and the problem of venting the exhaust.

The first step was to determine the required input and output of an electric motor to be used as the helicopter power plant. The first analysis was done using just the momentum method. This method calculates the power based on an exchange of energy between the rotor disk and the wake. The thrust required to hover the helicopter is related to this change in momentum between

the rotor disk and the wake below. First the expression for the thrust is presented in equation 1. This equation related the thrust to the change in mass flow rate from above the rotor disk v_0 (equal to zero) to below the rotor disk v_2 .

$$\text{Thrust} = (\text{mass/sec}) * (\text{Change in Flow Velocity})$$

$$\text{Thrust} = (\rho v_1 A) * (v_2 - v_0)$$

$$v_2 = \text{Velocity below the rotor disk} \quad \text{Eq (1)}$$

$$v_1 = \text{Velocity at the rotor disk}$$

$$v_0 = \text{Velocity above the rotor disk} \Rightarrow 0$$

Once, the expression for thrust has be determined the relationship between the flow velocity at the disk v_1 and the flow velocity below the rotor in the wake v_2 must be established. This relationship is established by equating the energy absorbed by the wake to the energy dissipated by the rotor.

$$\text{Energy Dissipated by Rotor} =$$

$$\text{Energy Absorbed by Wake}$$

$$\frac{E_R}{\text{sec}} = \frac{E_W}{\text{sec}} \quad \text{Eq (2)}$$

$$T * v_1 = \frac{1}{2} \left(\frac{\text{mass}}{\text{sec}} \right) (v_2)^2$$

$$(\rho v_1 A v_2) v_1 = \frac{1}{2} (\rho v_1 A) (v_2)^2$$

$$v_2 = 2 v_1$$

The expression for the inflow velocity v_1 in equation 2 is then substituted into the thrust expression in equation 1. Since the thrust to hover must equal the weight of the helicopter the thrust value is a known quantity and the only unknown is the inflow velocity v_1 . Rearranging the terms and solving for the inflow velocity (equation 3) illustrates the relationship of inflow to disk loading.

$$T = 2 \rho (v_1)^2 A$$

$$v_1 = \sqrt{\frac{T}{2 \rho A}}$$

$$v_1 = \left(\sqrt{\frac{T}{2 \rho}} \right) (\sqrt{DL})$$

$$DL = \frac{T}{A} \quad \text{Eq (3)}$$

The inflow velocity is related to the square root of the disk loading. For the helicopter used in this program the disk loading is 0.75 pound per square foot and the inflow velocity is 12.6 feet per second.

$$\begin{aligned}
T &= 12 \text{ [lbs]} \\
A &= 15.9 \text{ [ft}^2\text{]} \\
DL &= 0.75 \left[\frac{\text{lbs}}{\text{sqft}} \right] \\
v_1 &= 12.6 \left[\frac{\text{ft}}{\text{sec}} \right] \\
v_2 &= 25.2 \left[\frac{\text{ft}}{\text{sec}} \right]
\end{aligned}
\tag{Eq (4)}$$

The induced power required which is equal to the product of thrust and inflow velocity can then be calculated. The power value based on a figure of merit or efficiency of 60% for this helicopter is 341 watts (watts will be the unit for power since the power plant for this helicopter is an electric motor)

$$\begin{aligned}
h_{pi} &= \frac{T \sqrt{DL}}{550 \sqrt{2\rho}} = 0.2743 \text{ hp} = 205 \text{ watts} \\
h_{pa} &= \frac{h_{pi}}{\text{Figure of Merit}} \\
h_{pa} &= \frac{205}{0.6} = 341 \text{ watts}
\end{aligned}
\tag{Eq (5)}$$

The blade element method was then applied to the rotor system to improve the prediction of power required by the electric power plant. In this method the rotor blade is divided into segments or elements and lift and drag are calculated on each section using two dimensional airfoil characteristics. The results are then summed from the blade root to the blade tip to determine the thrust. The first quantity needed is the lift equation 6 is an expression for the lift on a single blade element.

$$\begin{aligned}
\Delta L &= q c_l c \Delta r \\
q &= \text{Local Dynamic Pressure} \\
q &= \frac{1}{2} \rho (\Omega r)^2 \\
c_l &= a \alpha \\
\alpha &= \theta - \phi \\
c_l &= a \left(\theta - \frac{v_1}{\Omega r} \right) \\
\Delta L &= \frac{1}{2} \rho (\Omega r)^2 a \left(\theta - \frac{v_1}{\Omega r} \right) c \Delta r
\end{aligned}
\tag{Eq (6)}$$

This expression is then integrated (equation 7) over the blade span to determine the thrust. The blades used in this program have no twist ($q = q_0$ "Collective Input") and have no taper.

$$\text{Thrust} = b \int_{R_1}^{R_2} \left(\frac{1}{2} \rho (\Omega r)^2 a \left(\theta - \frac{v_1}{\Omega r} \right) c \right) dr
\tag{Eq (7)}$$

In coefficient form the thrust for this helicopter is given in equation 8. To non-dimensionalize the thrust is divided by the air density (ρ) the rotor disk area (A) and the tip speed squared (ΩR^2). The thrust coefficient base on the effective rotor disk area (σA) is also given. Where s is the rotor solidity.

$$\begin{aligned}
\rho &= 0.002378 \left[\frac{\text{slugs}}{\text{sec}^3} \right] \\
\Omega &= 146.61 \left[\frac{\text{Rad}}{\text{sec}} \right] \\
C_T &= \frac{\text{Thrust}}{\rho A (\Omega R)^2} \\
\sigma &= \text{Solidity} = \frac{A_B}{A} = \frac{b c}{\pi R} \text{ (Constant Chord)} \\
\sigma &= 0.0589 \\
C_T/\sigma &= 0.0526
\end{aligned}
\tag{Eq (8)}$$

Once the expression for thrust has been determined it can be rearranged to show the function relationship between thrust and collective (equation 9). In this equation the term f is defined as the square root of one half the trust coefficient. The term f is physically the reduction in pitch angle q due to the orientation of the inflow velocity.

Based on the thrust of 12 pounds the collective angle would have to be 6.5° .

$$\begin{aligned}
\text{Thrust} &= b \left[\frac{\rho}{2} (\Omega R)^2 \right] a \left[\theta \left(\frac{R}{2} \right) - \phi_T \left(\frac{R}{2} \right) \right] c \\
\phi_T &= \frac{v_1}{\Omega R} \\
v_1 &= \sqrt{\frac{T}{2\rho A}} \\
\phi_T &= \sqrt{\frac{C_T}{2}} \\
T &= c b \left[\frac{\rho}{2} (\Omega R)^2 \right] a \left(\frac{R}{2} \right) \left[\theta \left(\frac{2}{3} \right) - \sqrt{\frac{C_T}{2}} \right] \\
C_T/\sigma &= \left(\frac{3}{4} \right) \left[\theta \left(\frac{2}{3} \right) - \sqrt{\left(\frac{\sigma}{2} \right) \left(\frac{C_T}{\sigma} \right)} \right] \\
\theta &= \left(\frac{3}{2} \right) \left[\left(\frac{3}{4} \right) \left(\frac{C_T}{\sigma} \right) + \sqrt{\left(\frac{\sigma}{2} \right) \left(\frac{C_T}{\sigma} \right)} \right]
\end{aligned}
\tag{Eq (9)}$$

The torque and power relationships are the final equation (equation 10). Where power is just the torque times the angular velocity. The torque is composed of two part one due to induced drag effects and one due to profile drag effects.

$$\begin{aligned} \Delta P &= \Delta Q \Omega \\ \Delta Q &= r (\Delta L \phi + \Delta D_o) \\ \Delta Q &= r (\{ [\frac{1}{2} \rho (\Omega r)^2] a (\theta - \phi) \\ &\quad + \{ [\frac{1}{2} \rho (\Omega r)^2] c_d \} \\ c_{Q/o} &= (1/4) [\theta (2/3) - \phi] \phi + c_{d/8} \\ C_Q &= C_T \sqrt{C_T/2} + \sigma c_{d/8} \\ C_P &= C_Q = 0.0002 \\ P &= C_P \rho A (\Omega r)^3 \end{aligned} \quad \text{Eq (10)}$$

From this equation the required power is 622 watts which is almost double that calculated by the momentum method. The calculation of power required by both these methods assumed a constant chord blade with no twist and no control surface.

The final method used to calculate the power required was a combined momentum - blade element method. There are two basic equations associated with the approach. These equations are

$$\Delta T = b (\rho/2) (\Omega r)^2 a (\theta - \phi) c \Delta r \quad \text{Eq (11)}$$

$$\Delta T = 4 \rho (v_1)^2 r \Delta r \quad \text{Eq (12)}$$

Equation 11 is the thrust developed according to the blade element theory and equation 12 is the thrust developed according to the momentum theory. These two are then set equal to each other and the result is a formula for the induced velocity.

$$\begin{aligned} 4 \rho (v_1)^2 r \Delta r &= b (\rho/2) (\Omega r)^2 a (\theta - \phi) c \Delta r \\ \phi &= \frac{v_1}{\Omega r} = \frac{a\sigma}{16(\Omega R)} \left[-1 + \sqrt{1 + \frac{32b(\Omega R)}{a\sigma}} \right] \\ \text{For cambered airfoils: } \theta &= \theta_o + \alpha_{0L} \\ \theta_o &\equiv \text{Collective Input} \\ \alpha_{0L} &\equiv \text{Angle of Attack @ Zero Lift} \end{aligned} \quad \text{Eq (13)}$$

Once the induced velocity is known the inflow angle can be determined

$$\phi = \frac{v_1}{\Omega r} \quad \text{Eq (14)}$$

and then substitution of equation 14 into equation 11 and integration from the blade root to the effective blade tip results in the thrust being developed by the rotor system.

$$\begin{aligned} T &= b \int_{R_1}^{R_2} (\rho/2) (\Omega r)^2 a (\theta - \phi) c dr \\ R_1 &\equiv \text{Start of Blade span accounting for root cutout} \\ R_2 &\equiv \text{End of Blade span accounting for tip loss} \\ B &\equiv \text{Tip loss} = 1 - 0.06/b = 0.97 \end{aligned} \quad \text{Eq (15)}$$

$$Q = b \int_{R_1}^{R_2} r \{ (\rho/2) (\Omega r)^2 a (\theta - \phi) c \} + \{ (\rho/2) (\Omega r)^2 c_d c \} dr$$

$$P = Q \Omega$$

Using these equations a parametric study was performed where the parameters were motor rpm (1300 rpm to 1500 rpm) and collective setting (3° to 7°) to determine if an electric motor could be found for this application. The results of this parametric study are listed in Table 1.

Based on these results and the size of the current internal combustion motor an electric motor with an output of 1200 watts (1.6 Horsepower) was selected. Although from Table 1 it would appear that this motor is very conservative it was selected because an actual value for the losses associated with the drive train and the power required for the tail rotor are unknown.

The helicopter airframe had to be modified and a mounting block had to be designed and fabricated to integrate the electric motor into the airframe. The motor mount was a rectangular block of aluminum with two orthogonal set screws to hold the electric motor and four mounting screws to mate with the mounting holes on the airframe. To achieve the proper alignment of the motor and the drive train the mounting holes located on the helicopter were elongated to allow longitudinal adjustment of the mounting block. In addition to the motor mount a coupler was also fabricated which

COLLECTIVE (DEGREES)		Rotor Angular Velocity (RPM)									
		1300		1350		1400		1450		1500	
		THRUST	POWER	THRUST	POWER	THRUST	POWER	THRUST	POWER	THRUST	POWER
3.0	3.4	2.2	3.8	2.4	4.0	2.7	4.2	3.0	4.5	3.3	
3.5	4.2	2.4	4.6	2.7	4.9	3.0	5.3	3.3	5.8	3.7	
4.0	5.1	2.7	5.6	3.0	6.0	3.3	6.4	3.7	6.8	4.1	
4.5	6.1	3.0	6.5	3.3	7.0	3.7	7.5	4.1	8.1	4.6	
5.0	7.0	3.3	7.5	3.7	8.1	4.1	8.7	4.6	9.3	5.1	
5.5	8.0	3.7	8.6	4.1	9.2	4.6	9.9	5.1	10.6	5.7	
6.0	9.0	4.1	9.7	4.6	10.4	5.1	11.2	5.7	12.0	6.3	
6.5	10.0	4.5	10.8	5.1	11.6	5.7	12.5	6.3	13.4	6.9	
7.0	11.1	4.9	11.9	5.6	12.8	6.2	13.8	6.9	14.7	7.7	

UNITS: THRUST = LBS POWER = WATTS/100

TABLE 1 Thrust and Power Output

allowed the motor to mate with the existing centrifugal clutch which is the first component of the drive train. These two components and the modification of the airframe mounting holes allowed the electric motor to be mated to the airframe.

Unlike the internal combustion motor which uses a throttle the electric motor requires an electronic speed controller. This device regulates the motor speed by adding or subtracting resistance from the input circuit which then decreases or increases voltage to the electric motor. The problem with this device is the removal of the heat generated by the electronics. This was not a trivial problem and during early ground tests of the helicopter a speed controller caught on fire and was destroyed. This problem was solved by locating the speed controller in the down wash of the main rotor. The device was moved and then a series of tests were performed where the speed setting was varied and using a temperature probe the controller temperature was measured after each test. This helped to locate the speed controller in the downwash where it would get sufficient cooling to run at any speed indefinitely. In addition to the new location a heat sink was added with fins to remove heat from the controller. The speed controller also was subject to overload once because of a voltage potential induced in the power tether cord. The voltage was a result of the long (60 foot) tether power cord used to provide power to the electric motor. This problem was solved by including a large capacitor (2200 μ f \ 50 volt) in the input power line to drain off the AC voltage before it could get to the speed controller. There also was a thermal problem

with the electric motor. This problem is not present when these motors are used in an airplane application because the downwash from the propeller is used to cool the motor but in our application the downwash is obstructed from cooling the motor. This problem was solved by attaching a cooling fan to the bottom output shaft of the motor and sucking air through the motor to provide sufficient cooling to keep the motor core below 300° F.

4.3 Helicopter Testing

A number of ground tests were performed on the basic system in order to determine electrical power requirements and limitations on the electric motor and motor speed control unit. Ground tests were also used to track and balance the main rotor blades. The process of balancing the blades is begun during fabrication of the blades when mass is added to the blades till they are of equal weight and spanwise center of gravity. The blades are then mounted in the blade cuffs of the rotor head and spun to see if they track in the same plan (tip path plan). The blades can be out of track for two reasons (1) improper balance (This will not be the reason if the balancing task was done correctly) and (2) there is a difference in pitch link length. These tests also were used to setup and make preliminary adjustments to the radio control unit and programming the radio to insure the proper spinup rate. The spinup rate is important to avoid ground resonance modes which can damage the helicopter electronics and to load the electric motor properly to avoid overheating the electric motor core. All these tests were performed using an unmodified blade (NACA 0012 with a 2.5 inch chord). The next series of tests were flight tests of the helicopter system with unmodified blades. The purpose of these tests were to provide the pilot with flight time with an electric powered helicopter and to refine the radio control unit setup. In addition to this, many mechanical problems were encountered which were not present during the ground spin tests. An example of one problem was the tendency for the gear teeth on the tail rotor

drive gear to strip during flights when the electric motor rpm would be slightly above the rpm developed by an internal combustion motor. This is a recurring problem since the motor speed control unit is very sensitive.

Results from these tests were an electric helicopter of this size can generate sufficient lift with the unmodified blades but care must be taken not to overheat the electric motor or the motor speed control unit. The main rotor speed during spinup on the ground was 1500 rpm and the hover rpm was 1400 rpm. The required battery voltage was 36 volts and there was a 10 volt drop in the 60 foot tether line between the batteries and the helicopter. The temperature developed by the electric motor was 150° F and the motor speed control was 120° F. These temperatures are near the upper operating limits for both these components.

The next test was a wind tunnel test to insure the structural integrity of the modified helicopter rotor blade. The standard blade was first modified by cutting a control surface into the blade. The control surface was located 4 inches from the tip of the blade, the spanwise length of the control surface was 8 inches and the chordwise length of the control surface was 40 percent of the airfoil chord or 1 inch. A plastic hinge was glued to the top surface of both the control surface and the blade to attach the two pieces. This configuration was then placed in the wind tunnel in a vertical orientation. The blade was subjected to a series of dynamic pressures minimum of 0 psf maximum of 50 psf. The pressure was increased to this maximum in 10 psf increments and was subjected to each dynamic pressure increment for approximately 10 minutes.

The results of this test were the modified blade demonstrated sufficient structural integrity for dynamic pressures from 0 to 50 psf and the control surface did not flutter.

The next test was to subject the modified rotor blade to a ground spin test to evaluate the structural integrity to centrifugal

load. For this test the helicopter was weighted with approximately 12 pounds of lead. The rotor was spun to 1600 rpm with zero collective input and was kept at this speed for approximately 5 minutes. Examination of the blade during the test showed no sign of vibration or flutter even though the blades did not track very well. After the test examination of the blades showed no structural integrity problems. The rotor was then spun up again and collective was applied in a controlled manner till the helicopter actually lifted off with the 12 pounds of ballast.

The results of this test were the modified blade demonstrated sufficient structural integrity for dynamic pressures from 0 to 180 psf and centrifugal loads associated with a rotational speed of 1600 rpm. Also under these conditions the control surface did not flutter.

The next flight tests were done with the modified blade using the conventional control system. In these tests the aircraft was hovered at 6 to 8 feet off the ground for approximately 5 minutes. This test was performed 8 times and in all flights the helicopter experienced only mechanical failures in the drive system. The major failure being the tendency for the gear teeth on the tail rotor drive gear to strip and we had one tail rotor blade strike on a hard landing during a gust. The purpose of these tests were also to provide the pilot with flight time with an electric powered helicopter with modified rotor blades.

The results of these test flights again emphasized the sensitivity of the drive system to overspeed problems. But the major outcome was the modified blades are able to lift the helicopter and can be controlled with conventional control inputs.

Ground tests of the helicopter with the modified blade activated to a camber change were the next set of tests performed. The objective of these was to demonstrate that a camber change could be maintained using the shape memory alloy actuation

system. These tests also gave the pilot some practice at activating and deactivating the control surface. The conditions for these tests were similar to the other ground tests where the rpm was varied from 0 to 1600 in increments of 100 and each increment was maintained for 5 minutes. Since the actuator wire was not directly exposed to the airstream, there was minimal aerodynamic cooling of the wire actuator and power requirements were low 1 amp at 3 volts.

The results of this test demonstrated the structural integrity of the shape memory alloy and the control surface actuation system.

The final test was a flight test of the helicopter where the shape memory actuator was activated and resulted in a vertical climb of the helicopter. This test was performed in the following sequence (1) the helicopter was hovered at 6 feet off the ground, (2) once a stable hover was achieved the actuator was activated and the helicopter climbed vertically with the pilot maintaining stability through cyclic and increased tail rotor pitch to overcome the additional torque placed on the main rotor system, (3) after a climb of 3 feet the pilot deactivated the actuator and varied the collective to land the helicopter.

The results of this test demonstrated the ability of the shape memory alloy actuator system to change blade camber. This camber change generated enough thrust to result in a vertical climb of the 8 pound helicopter. Therefore a shape memory alloy actuator system has the ability to effect the magnitude of camber changes required to replace the current collective control system on the helicopter.

4.4 Rotor Blade

A NACA 0012 is a standard main rotor blade cross section for this size helicopter. The blade span is 28 inches and the blade chordwise dimension is 2.5 inches resulting in a solidity of 0.0568. The design goal was to match the thrust generated at a collective setting greater than that required to

hover the helicopter by changing the camber of a portion of the rotor blade. The helicopter has an assumed weight of 12 pounds (actual weight 8 lbs.) therefore the cambered portion of the blade must generate thrust greater than 12 pounds of thrust for the helicopter to climb vertically. Assuming an increase in thrust of 4 pound what would be the required camber change of the airfoil? Blade element and momentum theory aerodynamics were used to determine the required collective setting to hover at 12 pounds. This value is 7° at 1450 rpm. Conservation of momentum was then used to determine the climb velocity V_N and is illustrated in Figure 8

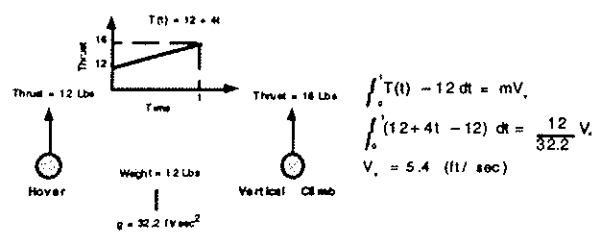


FIGURE 8 Vertical Climb Velocity

Once the climb velocity had been established, the size and location of the control surface had to be determined. The design methodology was to set the collective such that the helicopter would generate a thrust equal to the weight of the vehicle. The thrust generated by the control surface would then be employed for vertical climb or descent. Based on this methodology the collective was set at 7° which would generate 12 pounds of thrust which is enough for the helicopter to hover. Based on discussion with engineers at Kaman Aerospace Company the control surface was located at 75% of the span of the rotor blade. The dimensions of the control surface are 8 inches in the spanwise direction (28% of the total span) and 1 inch in the chordwise direction (40% of the total chord).

A 2D panel method airfoil analysis was performed to determine upper and lower airfoil section pressure distributions as well as sectional lift and drag coefficients. These coefficients were used to determine the incremental lift associated with rotor blade

segments and the resultant pressure distribution on the airfoil. The resultant pressure distribution is illustrated in Figure 9. From the pressure distribution illustrated in Figure 9 the effect of the deflected control surface can be seen as a sharp increase in the pressure differential at approximately 55% of the chord.

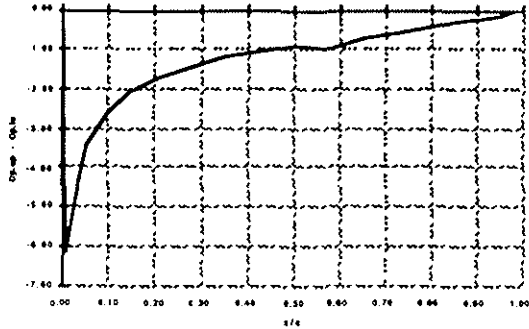


FIGURE 9 Airfoil Pressure Distribution

The area under this portion of the curve is the airload on the control surface and is used to calculate the required moment for deflecting the surface. Equation 16 is the integral for calculating the area and is equal to the lift coefficient for the control surface.

$$c_l = \frac{1}{c} \int_0^c C_{p_{lo}} - C_{p_{up}} dx \Rightarrow C \quad \text{Eq (16)}$$

Table 2 tabulates the incremental airloads on the control surface from the inside edge radius 1.5 feet to the outside edge at radius 2.08 feet.

The airload on the control surface is then the sum of the incremental airloads. This total lift then was assumed to act at the chordwise station of 1.83 inches from the leading edge or 0.33 inches aft of the hinge line. Based on these numbers the moment due to airloads to be overcome is 0.10 inch-pounds or 1.60 inch-ounces. Once the airload has been overcome the control surface must be deflected 4° for the effective angle of attack to be the required 9.88° . The geometric relationship between control

surface angle and effective angle of attack is illustrated in Figure 10.

Radius (Ft)	Velocity (Ft/Sec)	Dynamic Pressure (Lbs/SqFt)	Lift (Lbs)
1.42	215.33	55.13	0.03
1.50	228.00	61.81	0.03
1.58	240.67	68.87	0.04
1.67	253.33	76.31	0.04
1.75	266.00	84.13	0.05
1.83	278.67	92.33	0.05
1.92	291.33	100.92	0.06
Total Lift =>			0.30

TABLE 2 Control Surface Airload

Again estimating the lift by the combined blade element and momentum theories the total lift for this rotor system would be 16.5 pounds. Where the blades are set to a collective pitch of 7° and the control surface described above is deflected by 4° and the rotor is spinning at 1450 rpm. The actuation element used to manifest this deflection is a Shape Memory Alloy.

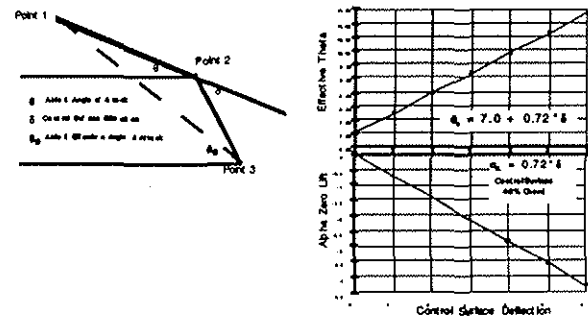


FIGURE 10 Effective Angle of Attack

The next issue to resolve was the power requirement for the SMA actuator element. Figure 11 illustrates the power required to activate a 2 inch long strand of 0.01 inch diameter SMA wire. This figure also illustrates that the shape memory effect can be used to deflect the control surface with a reasonable amount of electric power. Even though the time responses that one encounters when shape memory alloys are used for shape changes (1 hertz) are not as fast as the time responses with piezoelectric transducers a shape memory alloy can maintain the changed shape for a prescribed time duration. This makes the shape memory alloy an ideal smart or adaptive material for collective control.

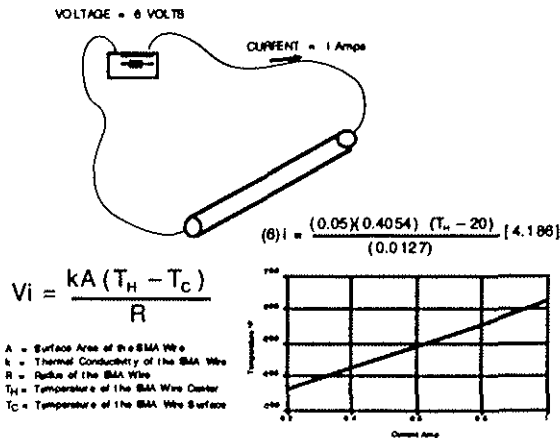


FIGURE 11 SMA Power vs. Temperature Relationship

Figure 12 illustrates the design configuration of the control surface and the shape memory alloy actuation element. Based on this figure when the SMA wire is heated it will contract pulling free end point "A" of the actuator lever arm forward. As the free end of the actuator lever arm moves forward the portion between points "B" and "C" will rotate clockwise and the embedded end point "D" of the control surface lever arm will move downward. The length of the actuator lever arm was based on the amount of strain recovery and force associated with this work. The amount of strain allowed in an application is a function of the number of cycles the material will experience this strain.

The manufacturers recommended strain for applications such as this is 4% and the available force is 6.5 ounces for SMA wire with a diameter of 0.010 inches. Since the required moment to be overcome is 5.44 inch-ounces the actuator lever arm (point "A" to "B") must be 0.84 inches in length. The 4% strain and a right angle pull orientation were then used to calculate the amount of SMA wire required and the voltage required. Figure 13 illustrates the layout of the SMA wire.

The 0.1" dimension shown in this figure represents the actual magnitude of the displacement at point "A" (free end of the

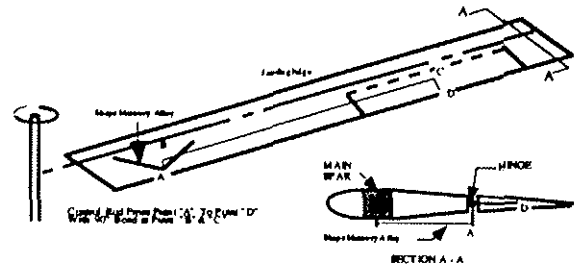


FIGURE 12 Adaptive Airfoil with Shape Memory Alloy

actuator lever arm). The required displacement from the calculations is 0.022" (0.84*Tan1.5°) which is a 0.9% strain.

$$R = r * L \Rightarrow 0.5W/in * 2.24in = 1.12W$$

$$V = R * i \Rightarrow 1.12W * 1A = 1.12V$$

$$P = V * i \Rightarrow 1.12V * 1A = 1.12W$$

The above calculation based on 4% strain being developed indicates that 1.12 watts per blade of power are required

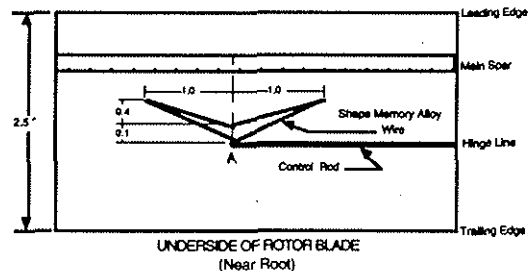


FIGURE 13 Actuator Wire Layout

Since only 0.9% strain is required and a 0.9% strain corresponds to a temperature of 60°F, the curve in Figure 11 would indicate that only 0.6 amps are required to power the actuator mechanism.

5.0 DEFLECTION OF SURFACE:

The scheme for providing a linear proportional control of the control surface had to be accomplished. The transmitter used in this project has four channels which have proportional control and one channel which has on / off control. The four proportional controls are as follows:

1. A mixed channel which controls motor speed and collective pitch
2. A channel which controls lateral cyclic pitch

3. A channel which controls longitudinal cyclic pitch
4. A channel which controls tail rotor collective pitch

Originally the on / off control channel transmitted a signal to a switch on the aircraft to provide power to the Shape Memory Alloy actuator. The power level was determined prior to the flight to be the amount of additional thrust needed for the vehicle to climb vertically. The next step was to devise a scheme by which the power to the actuator could be varied and thus change the control surface deflection in a proportional fashion while the vehicle was in flight.

The method devised to control the deflection of the control surface included the use of the on / off switch and the signal from the collective proportional channel. A relay was employed to switch the signal from the channel which normally controls the collective pitch and make it the channel which controlled the deflection of the control surface. Figure 14 illustrates the relay switch.

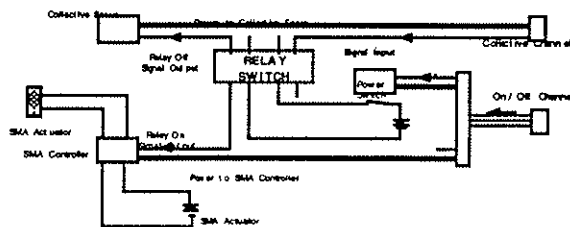


Figure 14. Relay switch

The relay switch illustrated above is the device which directs the signal from the collective channel. When the relay switch is in the off position the signal is passed to the collective servo for changing the rotor blade pitch. When the relay switch is in the on position the signal from the collective channel is directed to a controller which limits the power supplied to the SMA actuator.

The other component of this circuit is the power switch which turns the power on / off to the relay switch. This power switch is controlled by the on / off channel of the transmitter. Power from the on / off channel

is divided some being sent to the servo which activates the power switch and some being sent to the SMA controller. There are also two additional battery pack in the above figure. The first one provides power to the relay switch and is a 6 volt battery pack. The second provides power to the SMA actuator and is a 4.8 volt battery pack. The 4.8 volt battery pack was used in the original design to power the SMA actuator through the power switch which is controlled by the on / off channel.

The circuit now allows the operator to vary the control surface deflection by moving the stick which is normally associated with the collective control of the vehicle. Uninterrupted separate power sources are present to hold the position of the collective servo when the signal is directed to the SMA actuator or to maintain the control surface deflection when the signal is directed to the collective servo.

6.0 SUMMARY:

This research completes the preliminary design and proof of concept for a rotor which generates thrust through camber change. The design and testing of the new controller which allows the selection of any desired amount of control surface deflection has been completed and will be flown on the test helicopter soon. With the completion of the phase of work the next phase is ready to begin. The next phase will address the development of a sensor package to monitor the spanwise strain of the rotor blade. These two components are the basis for an intelligent rotor system which is the ultimate goal of this research.

7.0 REFERENCES:

- 1 Schetky, L.. "Shape Memory Alloys." *Scientific American*, 1 November 1979
- 2 Brown, W.. *Technical Characteristics of FLEXINOL*. Irvine California: Dynalloy, Inc.

- 3 Rogers,C.A. and Barker,D.K..
"Experimental Studies of Active Strain Energy Tuning of Adaptive Composites." In *31st AIAA Structures, Structural Dynamics and Materials Conference.* , 1990.
- 4 Rogers,C.A.. "Novel Design Concepts Utilizing Shape Memory Alloy Reinforced Composites." In *American Society of Composites 3rd Technical Conference on Composite Materials.* Lancaster, Pennsylvania: Technomic, 1988.
- 5 Rogers,C.A. and Robertshaw,H.H..
"Shape Memory Alloy Reinforced Composites." *Engineering Science Reprints 25, ESP25.88027,* (1988).
- 6 Nagaya,K., Takeda,S., Tsukui,Y. and Knmaido,Y.. "Active Control Method for Passing Through Critical Speeds of Rotating Shafts by Changing Stiffness of the Supports with Use of Memory Metals." *Journal of Sound & Vibration,* 113 (1987).
- 7 Baz,A., Ro,J., Poh,S. and Gilheany,J..
"Control of Smart Traversing Beam." In *Active Materials & Adaptive Structures.* Philadelphia, Pennsylvania: IOP Publishing Ltd., 1991.
- 8 Lagoudas,D.C. and Tadjbakhsh,I.G..
"Active Flexible Rods with Embedded SMA Fibers." In *Active Materials & Adaptive Structures.* Philadelphia, Pennsylvania: IOP Publishing Ltd., 1991.
- 9 Baz,A.,Inman,K. and McCoy,J..
"Active Control of Flexible Beams using Shape Memory Actuators." *Journal of Sound & Vibration,* 140 (1990).
- 10 Johnson, W., *Helicopter Theory,* Princeton University Press ,New Jersey, 1980.
- 11 Gessow, A. and Myers, G.C., Jr., *Aerodynamics of the Helicopter 8th Edition,* pp 29, Fredrick Ungar Publishing Co.,New York, 1985.
- 12 Roglin, R.L. and Hanagud, S.V.,1992,Shape Memory Alloy Camber Control,Patent Issued.
- 13 Hanagud, S.V. and Roglin, R.L., "Adaptive Airfoils", Souteastern Confrence of Theoretical and Applied Mechanics, 1992.
- 14 Hanagud, S.V., Roglin, R.L. and Nagesh Babu, G.L., "Smart Airfoils for Helicopter Control", Eighteenth European Rotorcraft Form, 1992.